Inorganic Chemistry

ARTICLE

pubs.acs.org/IC

Theoretical Analysis of Mechanistic Pathways for Hydrogen Evolution Catalyzed by Cobaloximes

Brian H. Solis and Sharon Hammes-Schiffer*

Department of Chemistry, 104 Chemistry Building, Pennsylvania State University, University Park, Pennsylvania 16802, United States

Supporting Information

ABSTRACT: The mechanistic pathways for hydrogen evolution catalyzed by cobalt complexes with supporting diglyoxime ligands are analyzed with computational methods. The cobaloximes studied are $Co(dmgBF_2)_2$ (dmg = dimethylglyoxime) and $Co(dpgBF_2)_2$ (dpg = diphenylglyoxime) in acetonitrile. The reduction potentials and pK_a values are calculated with density functional theory in conjunction with isodesmic reactions, incorporating the possibility of axial solvent ligand loss during the reduction process. The solvent reorganization energies for electron transfer between the cobalt complex and a metal electrode and the inner-sphere reorganization energies accounting for intramolecular rearrangements and the possibility of ligand loss are also calculated. The relative reduction potentials agree quantitatively with the available experimental values. The pK_as and reorganization energies agree qualitatively with estimates based on experimental data. The calculations suggest that a peak measured at ca. −1.0 V vs SCE in cyclic voltammetry experiments for $Co(dmgBF_2)_2$ is more likely to correspond to the $Co^{II}H/Co^{I}H$ reduction potential than the $Co^{III}H/Co^{II}H$ reduction potential. The calculations also predict pK_a values of Co−hydride complexes and reduction potentials for both cobaloximes that have not been determined experimentally. The results are consistent with a mechanism in which the Co(III) and Co(II) complexes have two axial solvent ligands and the Co(I) complex has a single axial ligand along the reaction pathway. Analysis of the free energy diagrams generated for six different monometallic and bimetallic hydrogen production pathways identified the most favorable pathways for $Co(dmgBF_2)_2$ and tosic acid. The thermodynamically favored monometallic pathway passes through a Co(III)H intermediate, and Co(II)H reacts with the acid to produce H_2. The thermodynamically favored bimetallic pathways also pass through the Co(III)H intermediate, but the pathways in which two Co(III)H or two Co(II)H complexes react to produce H_2 are not thermodynamically distinguishable with these methods. On the basis of the electrostatic work term associated with bringing the two cobalt complexes together in solution, the preferred bimetallic pathway involves the reaction of two Co(III)H complexes to produce H_2. This mechanistic insight is important for designing more effective catalysts for solar energy conversion.

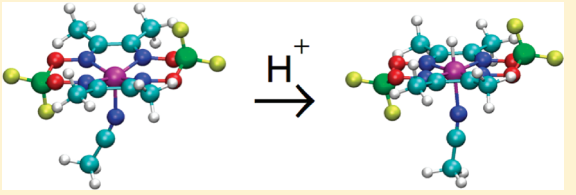

I. INTRODUCTION

Development of hydrogen evolution catalysts from earth-abundant materials is of great interest because such catalysts play a key role in proposed solar-driven water-splitting devices. Cobalt complexes with supporting diglyoxime ligands are among the promising candidates for robust and efficient hydrogen evolution catalysts. Specifically, $Co(dmgBF_2)_2$ (dmg = dimethylglyoxime) and $Co(dpgBF_2)_2$ (dpg = diphenylglyoxime) complexes have been shown to produce molecular hydrogen from protic solutions at relatively modest overpotentials.[1−4] Mechanistic studies indicate the presence of a Co(III)−hydride intermediate in several possible monometallic and bimetallic pathways, as summarized in Scheme 1.[1−12] The relative probabilities of these various mechanistic pathways depend on the strength and concentration of the acid as well as the redox properties of the cobaloxime. Although these cobaloxime catalysts have been studied experimentally with a broad spectrum of electrochemical and photochemical methods,[1−13] they have not been explored extensively with theoretical methods.

The objective of this paper is to use computational methods to investigate the properties of the $Co(dmgBF_2)_2$ and $Co(dpgBF_2)_2$ catalysts and to analyze the mechanistic pathways for hydrogen evolution catalyzed by $Co(dmgBF_2)_2$. A variety of computational methods have been developed for calculation of reduction potentials and pK_a values in these types of systems.[14−18] Our strategy for calculating reduction potentials and pK_a values is based on density functional theory (DFT) in conjunction with isodesmic reactions[15] utilizing experimentally studied reference complexes. In addition to providing accurate relative free energies, the isodesmic reactions are also used to incorporate the possibility of the dissociation of a solvent ligand during the reduction process. The outer-sphere (solvent) reorganization energies for electron transfer between a molecule and a metal electrode are calculated using DFT with a dielectric continuum model.[19] The inner-sphere (solute) reorganization energies for electron transfer are calculated using DFT for the gas phase reduced and oxidized species at equilibrium and nonequilibrium geometries.[20] Additional calculations are performed to estimate the inner-sphere reorganization energy associated with solvent ligand loss during certain electron transfer steps.[21,22] Marcus theory[23,24] can be used to estimate free energy barriers for the electron transfer steps.

Received: August 23, 2011
Published: September 26, 2011

Scheme 1. Monometallic (A) and Bimetallic (B) Pathways

Pathway 1

$$Co(II) + e^- \rightarrow Co(I)^-$$

$$Co(I)^- + HA \rightarrow Co(III)H + A^-$$

A: $Co(III)H + HA \rightarrow Co(III)^+ + A^- + H_2$

A: $Co(III)^+ + e^- \rightarrow Co(II)$

B: $2Co(III)H \rightarrow 2Co(II) + H_2$

Pathway 2

$$Co(II) + e^- \rightarrow Co(I)^-$$

$$Co(I)^- + HA \rightarrow Co(III)H + A^-$$

$$Co(III)H + e^- \rightarrow Co(II)H^-$$

A: $Co(II)H^- + HA \rightarrow Co(II) + A^- + H_2$

B: $2Co(II)H^- \rightarrow 2Co(I)^- + H_2$

B: $2Co(I)^- \rightarrow 2Co(II) + 2e^-$

Pathway 3

$$Co(II) + e^- \rightarrow Co(I)^-$$

$$Co(I)^- + e^- \rightarrow Co(0)^{2-}$$

$$Co(0)^{2-} + HA \rightarrow Co(II)H^- + A^-$$

A: $Co(II)H^- + HA \rightarrow Co(II) + A^- + H_2$

B: $2Co(II)H^- \rightarrow 2Co(I)^- + H_2$

B: $2Co(I)^- \rightarrow 2Co(II) + 2e^-$

Analysis of the energetics for the proposed mechanisms allows us to identify the most probable hydrogen production mechanisms for the cobaloxime catalysts under various experimental conditions. We compare our calculated reduction potentials of the $Co(dmgBF_2)_2$ and $Co(dpgBF_2)_2$ catalysts to the available experimental data and predict the reduction potentials of the Co−hydride complexes to assist in the interpretation of ambiguous electrochemical data.[4] We also predict the pK_a values for the Co−hydride species and compare to values estimated from simulated electrochemical data for the $Co(dmgBF_2)_2$ catalysts.[5] Our calculations of the reduction potentials with and without axial solvent ligands provide mechanistic insight regarding the presence and absence of these ligands along the reaction pathway. In addition, our calculated solvent and solute reorganization energies, in conjunction with the reaction free energies, provide information about the relative free energy barriers of the electron transfer steps. Comparison of the resulting free energy diagrams for the proposed mechanistic pathways enables identification of the most favorable pathways for a specified acid strength and overpotential.

An outline of this paper is as follows. Section II presents the theoretical methods used for calculation of reduction potentials, pK_as, reaction free energies, reorganization energies, and electron transfer free energy barriers. Application of these methods to the hydrogen evolution pathways proposed for the cobaloxime catalysts and analysis of the relative probabilities of these pathways are presented in section III. The conclusions of this work are summarized in section IV.

II. THEORETICAL METHODS

In this section, we discuss the methods used for calculation of reduction potentials, pK_as, reaction free energies, reorganization energies, and electron transfer free energy barriers. In section II.A., we present the methodology used to calculate reduction potentials and pK_as, as well as the computational details for the results presented in this paper. In section II. B., we describe the strategies for calculating the inner-sphere (solute) and outer-sphere (solvent) reorganization energies to estimate the free energy barriers for electron transfer.

II.A. Reduction Potentials and pK_as. The Born−Haber cycle allows us to express the reaction free energy for reduction of a molecule in solution in terms of the reaction free energy for reduction of the molecule in the gas phase, $\Delta G^{o,redox}_{gas}$, and the solvation free energies of the reduced and oxidized species, $\Delta G^o_s(\mathrm{Red})$ and $\Delta G^o_s(\mathrm{Ox})$, respectively[25]

$$\Delta G^{o,\,redox}_{solv} = \Delta G^{o,\,redox}_{gas} + \Delta G^o_s(\mathrm{Red}) - \Delta G^o_s(\mathrm{Ox}) \quad (1)$$

The gas-phase reaction free energy is calculated as

$$\Delta G^{o,\,redox}_{gas} = \Delta H^{o,\,redox}_{gas} - T\Delta S^{o,\,redox}_{gas} \quad (2)$$

where the enthalpy includes contributions from zero-point energy, the entropic contribution is calculated from the vibrational frequencies, and the temperature is T = 298.15 K. The reduction potentials are calculated with the Nernst equation, $E^\circ = -\Delta G^{o,redox}_{solv}/F$, where F is the Faraday constant.

The Born−Haber cycle is also used for calculation of pK_as.[26] In this case, the reaction free energy for deprotonation of a molecule in solution is expressed in terms of the reaction free energy for deprotonation of the molecule in the gas phase, $\Delta G^{o,pK_a}_{gas}$, and the solvation free energies of the acid, conjugate base, and proton, $\Delta G^o_s(\mathrm{AH})$, $\Delta G^o_s(\mathrm{A}^-)$, and $\Delta G^o_s(\mathrm{H}^+)$, respectively

$$\Delta G^{o,\,pK_a}_{solv} = \Delta G^{o,\,pK_a}_{gas} + \Delta G^o_s(\mathrm{A}^-) + \Delta G^o_s(\mathrm{H}^+) - \Delta G^o_s(\mathrm{AH}) \quad (3)$$

As for reduction, the gas-phase reaction free energy is calculated from eq 2. The pK_a is calculated from the reaction free energy with the standard relation, $pK_a = \Delta G^{o,pK_a}_{solv}/[\ln(10)RT]$. In our procedure, the contribution of $\Delta G^o_s(\mathrm{H}^+)$ to $\Delta G^{o,pK_a}_{solv}$ does not affect the final value for the pK_a because of the cancellation in the isodesmic reactions described below. All reduction potentials and pK_as are calculated in acetonitrile in this paper because the majority of the relevant electrochemical experiments have been performed in acetonitrile, although some have been carried out in other solvents. Note that self-consistent pK_a scales of acidity have been defined in nonaqueous solutions such as acetonitrile, but the acidities determined in different solvents are not directly comparable.[27]

The free energies calculated with the Born−Haber cycle are used in isodesmic reactions with appropriate references to account for systematic computational error. Typically direct DFT calculations of reduction potentials and pK_as are not sufficiently accurate due to limitations in the basis sets and electron exchange-correlation functionals. Use of isodesmic reactions with appropriate references has been shown to account for these systematic errors and hence to provide quantitatively accurate reduction potentials and pK_as.[15] In addition, this strategy avoids the necessity of determining quantities such as the free energies of the gas-phase electron and proton and the solvation free energy of the proton, which have been discussed in the literature,[14,16,28] due to cancellation of these quantities in the isodesmic reactions. These cancellations in the isodesmic reactions also allow us to include the effects of solvent ligand loss

dx.doi.org/10.1021/ic201842v |Inorg. Chem. 2011, 50, 11252–11262

without calculating the free energy of self-solvation for the ligand.[14]

Four reference reactions, including reductions and a deprotonation, are used in the isodesmic reactions

$$\begin{aligned}
&\text{A}: \quad \mathrm{Co^{II}(dmgBF_2)_2L_2 + e^- \rightarrow Co^{I}(dmgBF_2)_2L^- + L} \\
&\qquad E^{\circ}_{\mathrm{RefA}} = -0.55 \text{ V vs SCE} \\
&\text{B}: \quad \mathrm{Co^{II}(dppe)_2L^{2+} + e^- \rightarrow Co^{I}(dppe)_2^+ + L} \\
&\qquad E^{\circ}_{\mathrm{RefB}} = -0.32 \text{ V vs SCE} \\
&\text{C}: \quad \mathrm{Co^{I}(dppe)_2^+ + e^- \rightarrow Co^{0}(dppe)_2} \\
&\qquad E^{\circ}_{\mathrm{RefC}} = -1.18 \text{ V vs SCE} \\
&\text{D}: \quad \mathrm{Co^{III}H(dmgBF_2)_2L \rightarrow Co^{I}(dmgBF_2)_2L^- + H^+} \\
&\qquad \mathrm{p}K_{\mathrm{a}}(\mathrm{RefD}) = 13.3
\end{aligned} \tag{4}$$

where A is a reduction of a cobaloxime, $Co(dmgBF_2)_2$, B is a reduction of the reference molecule $Co(dppe)_2$ [dppe = bis-(diphenylphosphino)ethane] that includes ligand loss, C is a reduction of this reference molecule without ligand loss, and D is a deprotonation of a cobaloxime. Note that the molecules of interest have two $dmgBF_2$ or $dpgBF_2$ ligands, while some reference molecules have two dppe ligands. Moreover, L is an axial acetonitrile ligand, which can be lost to bulk solvent upon reduction. Reference reactions A, B, and D include the loss of an acetonitrile ligand or an acidic proton, which will cancel in the isodesmic reactions presented below. The justification for assuming the axial ligand loss in the reference reaction A is given below in the analysis of the reduction potentials for the cobaloximes. The assumption of ligand loss in reference reaction B is based on the analysis in ref 29. The reduction potentials and pK_a for these reference reactions were determined experimentally: the reduction potential for reference A was obtained from ref 4, the reduction potentials for references B and C were obtained from ref 29, converting from the ferrocenium/ferrocene (Fc^+/Fc) reference to the saturated calomel electrode (SCE) reference with a shift of 0.38 V,[30,31] and the pK_a for reference D was obtained from ref 5. Note that this reference pK_a was not obtained by a direct experimental measurement but rather was determined from simulations of electrochemical cyclic voltammograms.[5]

The first isodesmic reaction is used to account for the differences between the $dmgBF_2$ and the dppe ligands for reduction potentials because the other reference reactions contain the dppe ligands. This isodesmic reaction is the difference between reactions B and A in eq 4, leading to

$$\mathrm{Co^{I}(dmgBF_2)_2L^- + Co^{II}(dppe)_2L^{2+} \rightarrow Co^{II}(dmgBF_2)_2L_2 + Co^{I}(dppe)_2^+} \tag{5}$$

The free energy corresponding to the systematic computational error for this reaction is

$$\Delta G_{\mathrm{r}}^{\circ,\mathrm{A/B}} = -\Delta G_{\mathrm{r}}^{\circ} + FE^{\circ}_{\mathrm{RefA}} - FE^{\circ}_{\mathrm{RefB}} \tag{6}$$

where $\Delta G_{\mathrm{r}}^{\circ}$ is the free energy of reaction for eq 5, as calculated by the Born−Haber cycle, and $E^{\circ}_{\mathrm{RefA}}$ and $E^{\circ}_{\mathrm{RefB}}$ are the experimental reduction potentials for reference reactions A and B, respectively. All subsequent isodesmic reactions for reduction potentials will inherently contain eq 6 via addition of $\Delta G_{\mathrm{r}}^{\circ,\mathrm{A/B}}$ to account for systematic errors arising from differences between the dppe ligands in the reference molecules and the $dmgBF_2$ ligands in the cobaloximes. This procedure can be viewed as employing a double isodesmic reaction for each of the reduction processes described below. A single isodesmic reaction using reference reaction D was used for the pK_a calculations. The isodesmic reactions and the resulting equations for the reduction potentials and pK_as are given in Table 1.

The reduction potentials and pK_as calculated with the equations in Table 1 are used to determine the relative free energies for the pathways given in Scheme 1. The following thermodynamic cycle is used to calculate the free energy for the hydrogen production step of Pathway 1A

$$\begin{aligned}
&\text{A}': \quad \mathrm{HA \rightarrow A^- + H^+} \\
&\qquad \ln(10)RT[\mathrm{p}K_{\mathrm{a}}(\mathrm{HA})] \\
&\text{B}': \quad \mathrm{Co(III)H \rightarrow Co(I)^- + H^+} \\
&\qquad \ln(10)RT[\mathrm{p}K_{\mathrm{a}}(\mathrm{Co^{III}H})] \\
&\text{C}': \quad \mathrm{Co(I)^- \rightarrow Co(II) + e^-} \\
&\qquad FE^{\circ}_{\mathrm{Co^{II}/Co^{I}}} \\
&\text{D}': \quad \mathrm{Co(II) \rightarrow Co(III)^+ + e^-} \\
&\qquad FE^{\circ}_{\mathrm{Co^{III}/Co^{II}}} \\
&\text{E}': \quad \mathrm{2H^+ + 2e^- \rightarrow H_2} \\
&\qquad -2FE^{\circ}_{\mathrm{H^+/H_2}} \\
&\text{F}': \quad \mathrm{Co(III)H + HA \rightarrow Co(III)^+ + A^- + H_2} \\
&\qquad \Delta G_{\mathrm{r}}^{\mathrm{H_2}}
\end{aligned} \tag{7}$$

where the reaction given in F′ is the sum of the reactions given in A′−E′ and $\Delta G_{\mathrm{r}}^{\mathrm{H_2}}$ is the sum of the free energies corresponding to these five reactions. $E^{\circ}_{\mathrm{H^+/H_2}}$ is the reduction potential for $H^+ + e^- \rightarrow (1/2)H_2$ and has been determined to be $E^{\circ}_{\mathrm{H^+/H_2}} = -0.14$ V vs Fc^+/Fc = 0.24 V vs SCE in acetonitrile.[4,30−33] Analogous thermodynamic cycles were employed in the calculation of the free energies for the hydrogen production steps in the other pathways.

These calculations were performed with DFT using Gaussian09.[34] The $Co(dmgBF_2)_2$ molecules were optimized in the gas phase at the B3P86/6-311+G** level of theory.[35−41] The $Co(dppe)_2$ and $Co(dpgBF_2)_2$ molecules were optimized at the same level of theory except the smaller basis set 6-31G was used for the phenyl rings.[42] The gas phase optimized structures for the $Co(dmgBF_2)_2$ molecules considered in this study are depicted in Figure 1. Solvation energies were calculated with the conductor-like polarizable continuum model (C-PCM)[43,44] using Bondi radii[45] and including nonelectrostatic interactions resulting from dispersion,[46,47] repulsion,[47] and cavity formation.[48] For comparison of the geometries in the gas phase and solution, the $Co(dmgBF_2)_2$ molecules were also optimized in the presence of the continuum solvent. The B3P86 functional with similar basis sets, the C-PCM solvent model, and isodesmic reactions involving a platinum reference compound were shown previously to predict hydricities with precisions of 2.0 kcal/mol, acidities with a precision of 1.9 pK_a units, and reduction potentials with precisions of 0.07 V for cobalt and nickel hydride complexes in acetonitrile.[15] For further benchmarking, we performed additional calculations with the B3LYP functional,[35,49] but these calculations did not reproduce the experimental geometries as accurately as did the B3P86 functional. These results are provided in Table S1, Supporting Information.

We tested the accuracy of our approach for calculation of reduction potentials of Co−hydride complexes by calculating the reduction potential for $Co^{II}H(dppe)_2^+ + e^- \rightarrow Co^{I}H(dppe)_2$ using a single isodesmic reaction with reference reaction C. Our calculated reduction potential of −0.83 V vs SCE is in excellent

dx.doi.org/10.1021/ic201842v |Inorg. Chem. 2011, 50, 11252–11262

Table 1. Isodesmic Reactions for Calculating Reduction Potentials and pK_as in Cobaloximes

process	isodesmic reaction	resulting equation[a]
$Co^{III}H(dmgBF_2)_2L + e^- \rightarrow Co^{II}H(dmgBF_2)_2^- + L$	$Co^{III}H(dmgBF_2)_2L + Co^{I}(dppe)_2^+ \rightarrow Co^{II}H(dmgBF_2)_2^- + Co^{II}(dppe)_2L^{2+}$	$E^o_{Co^{III}H/Co^{II}H} = \frac{-\Delta G_r^{o,A/B}}{F} - \frac{\Delta G_r^o}{F} + E^o_{RefB}$
$Co^{I}(dmgBF_2)_2L^- + e^- \rightarrow Co^{0}(dmgBF_2)_2^{2-} + L$	$Co^{I}(dmgBF_2)_2L^- + Co^{I}(dppe)_2^+ \rightarrow Co^{0}(dmgBF_2)_2^{2-} + Co^{II}(dppe)_2L^{2+}$	$E^o_{Co^{I}/Co^{0}} = \frac{-\Delta G_r^{o,A/B}}{F} - \frac{\Delta G_r^o}{F} + E^o_{RefB}$
$Co^{III}(dmgBF_2)_2L_2^+ + e^- \rightarrow Co^{II}(dmgBF_2)_2L_2$	$Co^{III}(dmgBF_2)_2L_2^+ + Co^{0}(dppe)_2 \rightarrow Co^{II}(dmgBF_2)_2L_2 + Co^{I}(dppe)_2^+$	$E^o_{Co^{III}/Co^{II}} = \frac{-\Delta G_r^{o,A/B}}{F} - \frac{\Delta G_r^o}{F} + E^o_{RefC}$
$Co^{II}H(dmgBF_2)_2^- + e^- \rightarrow Co^{I}H(dmgBF_2)_2^{2-}$	$Co^{II}H(dmgBF_2)_2^- + Co^{0}(dppe)_2 \rightarrow Co^{I}H(dmgBF_2)_2^{2-} + Co^{I}(dppe)_2^+$	$E^o_{Co^{II}H/Co^{I}H} = \frac{-\Delta G_r^{o,A/B}}{F} - \frac{\Delta G_r^o}{F} + E^o_{RefC}$
$Co^{II}H(dmgBF_2)_2^- \rightarrow Co^{0}(dmgBF_2)_2^{2-} + H^+$	$Co^{II}H(dmgBF_2)_2^- + Co^{I}(dmgBF_2)_2L^- \rightarrow Co^{0}(dmgBF_2)_2^{2-} + Co^{III}H(dmgBF_2)_2L$	$pK_a(Co^{II}H) = \frac{\Delta G_r^o}{\ln(10)RT} + pK_a(RefD)$

[a] ΔG_r^o for each equation is the free energy for the corresponding isodesmic reaction.

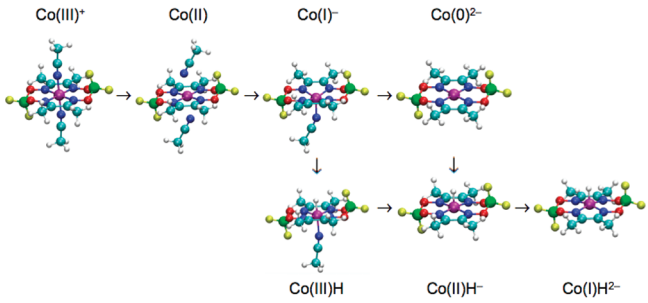

Figure 1. Gas phase optimized $Co(dmgBF_2)_2$ structures in various oxidation and protonation states. Horizontal arrows represent reduction, and vertical arrows represent protonation. Color scheme: purple, Co; blue, N; cyan, C; red, O; green, B; yellow, F; white, H.

agreement with the experimental value of −0.78 V vs SCE.[29] This agreement provides a degree of validation for the computational approach. Further validation is provided below by comparison to the experimental cobaloxime reduction potentials.

II.B. Reorganization Energies and Free Energy Barriers for Electron Transfer. According to Marcus theory, the free energy barrier for electron transfer is[20,21]

$$\Delta G^{\ddagger} = \frac{(\Delta G^o + \lambda_{tot})^2}{4\lambda_{tot}} \tag{8}$$

where the total reorganization energy λ_{tot} is the sum of the inner-sphere and solvent reorganization energies: $\lambda_{tot} = \lambda_i + \lambda_s$. In this subsection, we describe the methods for calculating these reorganization energies.

We calculated the heterogeneous solvent reorganization energies using a previously developed model in which the molecule is represented by a point charge at the center of a spherical cavity immersed in a dielectric continuum solvent near a metal electrode.[19] In our implementation, the spherical cavity is placed on the surface of the electrode, neglecting the double-layer effects. The radius of the sphere is chosen to reproduce the volume of the cavity obtained from the C-PCM calculations for these molecules. To compare with experimentally estimated reorganization energies for self-exchange reactions,[11] we calculated the homogeneous solvent reorganization energies for electron transfer self-exchange reactions of $Co(dpgBF_2)_2$ complexes using the analytical equation derived for two tangent spherical cavities of equal radius.[50] In our calculations, the radius of each spherical cavity was chosen to be the same as that used in the heterogeneous case. Note that the homogeneous solvent reorganization energy is approximately twice the magnitude of the heterogeneous solvent reorganization energy.[51]

We calculated the inner-sphere reorganization energy with the following expression[20]

$$\lambda_i = [U_{Ox}(Q_e^{Red}) - U_{Ox}(Q_e^{Ox}) + U_{Red}(Q_e^{Ox}) - U_{Red}(Q_e^{Red})]/2 \tag{9}$$

where Q_e^{Red} and Q_e^{Ox} are the equilibrium geometries of the reduced and oxidized species, respectively, and U_{Red} and U_{Ox} are the electronic energies for the reduced and oxidized species, respectively. As shown in the previous subsection, some of the reduction reactions involve the dissociation of an acetonitrile ligand. We account for the inner-sphere reorganization energy due to ligand loss with an approximate expression developed by

Savéant and co-workers[21,22]

$$\lambda_i^{\text{ligand loss}} = 4\Delta G^{\ddagger}_{\text{ligand loss}} \quad (10)$$

where $\Delta G^{\ddagger}_{\text{ligand loss}}$ is the barrier to dissociation of the ligand with all other nuclear coordinates fixed, assuming that $\Delta G^{\circ} = 0$ (see the example in Figure S1, Supporting Information). If the electron transfer and associated ligand loss occur by a concerted mechanism, the total inner-sphere reorganization energy is the sum of eq 10, which accounts for ligand loss, and eq 9, which accounts for the species in the absence of the ligand. If the mechanism is sequential, the inner-sphere reorganization energy for electron transfer does not include $\lambda_i^{\text{ligand loss}}$.

III. RESULTS AND DISCUSSION

III.A. Structures and Axial Ligands along the Reaction Pathway. To test the reliability of the computational methods, we compared the gas phase optimized geometries of Co(dmgBF$_2$)$_2$, Co(dpgBF$_2$)$_2$, and Co(dppe)$_2$ complexes to crystal structures for Co(dpgBF$_2$)$_2$ and Co(dppe)$_2$ complexes. The most relevant bond lengths and angles are compared in Tables 2 and 3. Table 2 illustrates that the presence of terminal phenyl instead of methyl groups on the oxime has a negligible impact on the distances of atoms directly bound to the cobalt center. The bond distances and angles for both Co(dmgBF$_2$)$_2$ and Co(dpgBF$_2$)$_2$ agree well with the crystal structure data for Co(dpgBF$_2$)$_2$, and the results for Co(dppe)$_2$ agree well with the crystal structure data for Co(dppe)$_2$, providing validation for the computational method. For the quantities examined in Tables 2 and 3, the calculated bond lengths are within 0.04 Å of the values in the crystal structures, and the calculated angles are within 3° of the values in the crystal structures. As shown in Table 2, additional optimizations of Co(dmgBF$_2$)$_2$ in solution indicate that solvation does not significantly alter the geometry.

Table 2. Comparison of Calculated and Experimental Bond Distances for Co(dmgBF$_2$)$_2$ and Co(dpgBF$_2$)$_2$[a]

		Co−N$_{\text{nitrile}}$	Co−N$_{\text{imine}}$
Co$^{\text{II}}$(dpgBF$_2$)$_2$L$_2$	experiment[b]	2.24	1.89
	DFT/B3P86 (gas)	2.26	1.89
Co$^{\text{II}}$(dmgBF$_2$)$_2$L$_2$	DFT/B3P86 (gas)	2.27	1.89
	DFT/B3P86 (C-PCM)	2.25	1.89
		Co−N$_{\text{nitrile}}$	Co−N$_{\text{imine}}$
Co$^{\text{I}}$(dpgBF$_2$)$_2$L$^-$	experiment[b]	1.97	1.85
	DFT/B3P86 (gas)	1.93	1.86
Co$^{\text{I}}$(dmgBF$_2$)$_2$L$^-$	DFT/B3P86 (gas)	1.94	1.86
	DFT/B3P86 (C-PCM)	1.95	1.86

[a] Values given in Angstroms. [b] Reference 4.

The presence or absence of axial solvent ligands in the cobaloximes cannot be directly determined experimentally in solution. X-ray crystal structures suggest that Co$^{\text{II}}$(dmgBF$_2$)$_2$ is an octahedron with two axial acetonitrile ligands, while Co$^{\text{I}}$(dmgBF$_2$)$_2^-$ is square pyramidal with one axial acetonitrile ligand.[4] In principle, Co$^{\text{II}}$(dmgBF$_2$)$_2$ could adopt a six-coordinate structure in the crystal structure due to packing constraints but adopt a different coordination in solution. Thus, we considered mechanisms with ligand structures that include Co$^{\text{II}}$(dmgBF$_2$)$_2$ as an octahedron with two axial acetonitrile ligands or a five-coordinated Co$^{\text{II}}$(dmgBF$_2$)$_2$ complex with only a single axial acetonitrile as follows

$$\text{Co(III)L}_2^+ \rightarrow \text{Co(II)L}_2 \rightarrow \text{Co(I)L}^- \rightarrow \text{Co(0)}^{2-} \quad (11)$$

$$\text{Co(III)L}_2^+ \rightarrow \text{Co(II)L} \rightarrow \text{Co(I)L}^- \rightarrow \text{Co(0)}^{2-} \quad (12)$$

$$\text{Co(III)L}_2^+ \rightarrow \text{Co(II)L} \rightarrow \text{Co(I)}^- \rightarrow \text{Co(0)}^{2-} \quad (13)$$

In all three mechanisms, Co$^{\text{III}}$(dmgBF$_2$)$_2^+$ is assumed be an octahedron with two axial acetonitrile ligands. During the geometry optimization of Co$^{\text{I}}$(dmgBF$_2$)$_2$L$_2^-$ (i.e., with two axial acetonitrile ligands), one of the ligands dissociated, so we did not consider the Co$^{\text{I}}$(dmgBF$_2$)$_2$L$_2^-$ complex in the above mechanisms. Similarly, optimization of Co^0(dmgBF$_2$)$_2^{2-}$ with one or two axial acetonitrile ligands resulted in dissociation of the axial ligand(s), so we did not consider Co^0(dmgBF$_2$)$_2$L^{2-} or Co^0(dmgBF$_2$)$_2$L$_2^{2-}$ in the above mechanisms. In principle, Co^0(dmgBF$_2$)$_2^{2-}$ could adopt a distorted tetrahedron structure, but in our calculations all molecules without axial ligands adopted the square planar geometry.

The reduction potentials calculated for the mechanisms in eqs 11 − 13 are provided in Table S2, Supporting Information. Since we used the isodesmic reaction in eq 5 as a reference for all isodesmic reactions, the calculated reduction potential, $E^{\circ}_{\text{Co}^{\text{II}}/\text{Co}^{\text{I}}}$, for Co(dmgBF$_2$)$_2$ agrees with experiment by construction. Comparison of the calculated reduction potential, $E^{\circ}_{\text{Co}^{\text{III}}/\text{Co}^{\text{II}}}$, for the mechanisms in eqs 11 − 13 to the experimental value indicates that the mechanism in eq 11 leads to the best agreement with experiment. The mechanisms in eqs 12 and 13 are ruled out because they lead to qualitatively incorrect values for the reduction potential $E^{\circ}_{\text{Co}^{\text{III}}/\text{Co}^{\text{II}}}$ (see Table S2, Supporting Information). Thus, we use the mechanism in eq 11 for analysis in the remainder of the paper. For the protonated cobalt complexes, five-coordinated Co$^{\text{I}}$(dmgBF$_2$)$_2$L$^-$ becomes six-coordinated Co$^{\text{III}}$H(dmgBF$_2$)$_2$L, as postulated in ref 4, and square planar Co^0(dmgBF$_2$)$_2^{2-}$ becomes five-coordinated Co$^{\text{II}}$H(dmgBF$_2$)$_2^-$. During the geometry optimization of Co$^{\text{II}}$H(dmgBF$_2$)$_2$L$^-$,

Table 3. Comparison of Calculated and Experimental Bond Distances and Angles for Co$^{\text{I}}$H(dppe)$_2$[a]

distances	Co−P1	Co−P2	Co−P3	Co−P4	Co−H
experiment[b]	2.15	2.12	2.16	2.15	1.46
DFT/B3P86 (gas)	2.18	2.13	2.17	2.17	1.48
angles	P1−Co−P2	P1−Co−P4	P2−Co−P3		P3−Co−P4
experiment[b]	87.0	107.7	123.4		91.1
DFT/B3P86 (gas)	87.1	104.6	121.9		91.9

[a] Bond distances given in Angstroms and angles in degrees. [b] Reference 29.

Table 4. Comparison of Calculated and Experimental Reduction Potentials of Cobaloximes[a]

		$E^{\circ}_{Co^{III}/Co^{II}}$	$E^{\circ}_{Co^{II}/Co^{I}}$	$E^{\circ}_{Co^{I}/Co^{0}}$	$E^{\circ}_{Co^{III}H/Co^{II}H}$	$E^{\circ}_{Co^{II}H/Co^{I}H}$
$Co(dmgBF_2)_2$	experiment[c]	~0.2	−0.55			
	DFT/B3P86	0.20	−0.55[b]	−0.94	−0.53	−1.25
$Co(dpgBF_2)_2$	experiment[c]	~0.3	−0.28			
	DFT/B3P86	0.26	−0.27	−0.85	−0.40	−1.07

[a] Values given in Volts vs SCE in acetonitrile. [b] $E^{\circ}_{Co^{II}/Co^{I}}$ for $Co(dmgBF_2)_2$ is used as a reference in the isodesmic reactions. [c] Reference 4. In the cyclic voltammetry experiments, $E^{\circ}_{Co^{III}/Co^{II}}$ is determined from an irreversible couple and $E^{\circ}_{Co^{II}/Co^{I}}$ is determined from a reversible couple.

Table 5. Comparison of Calculated and Experimental pK_as of Cobaloximes in Acetonitrile

		Co(III)H	Co(II)H
$Co(dmgBF_2)_2$	experimental[a]	13.3	23.0
	DFT/B3P86	13.3[b]	20.2
$Co(dpgBF_2)_2$	DFT/B3P86	8.9	16.3

[a] Reference 5. [b] The pK_a for $Co^{III}H(dmgBF_2)_2$ was used as a reference in the isodesmic reactions.

Table 6. Reorganization Energies for Electron Transfer Steps in $Co(dmgBF_2)_2$ Complexes[a]

	$Co^{III}L_2/Co^{II}L_2$	$Co^{II}L_2/Co^{I}L$	$Co^{I}L/Co^{0}$	$Co^{III}HL/Co^{II}H$	$Co^{II}H/Co^{I}H$
λ_i	1.01	0.46	0.26	0.27	0.30
$\lambda_i^{\text{ligand loss}}$		(0.55)	(0.61)	(0.53)	
λ_s[b]	0.41	0.42	0.45	0.44	0.45

[a] Values given in eV. [b] Heterogeneous solvent reorganization energies calculated for a spherical cavity in acetonitrile on the surface of an electrode.

the axial acetonitrile ligand dissociated, so we did not consider this complex in the mechanisms for hydrogen production.

III.B. Reduction Potentials and pK_as. A comparison of the calculated and experimental reduction potentials for the cobaloximes is provided in Table 4. As mentioned above, the reduction potential $E^{\circ}_{Co^{II}/Co^{I}}$ is identical to the experimental value by construction using the isodesmic reactions. The calculated value of $E^{\circ}_{Co^{III}/Co^{II}}$ = 0.20 V vs SCE for $Co(dmgBF_2)_2$, however, was calculated independently and is in excellent agreement with the experimental value of ~0.2 V vs SCE. Note that this experimental value was determined from an irreversible couple and therefore is not as reliable as the value for $E^{\circ}_{Co^{II}/Co^{I}}$, which was determined from a reversible couple. Moreover, in ref 4 another peak measured at ca. −1.0 V vs SCE was tentatively assigned to the reduction potential $E^{\circ}_{Co^{III}H/Co^{II}H}$ due to similar peaks that appear in related metal complexes. Our calculations suggest that this transition is more likely to correspond to the reduction potential $E^{\circ}_{Co^{I}/Co^{0}}$ or $E^{\circ}_{Co^{II}H/Co^{I}H}$. Since this peak was observed only in the presence of acid, we attribute this peak to $E^{\circ}_{Co^{II}H/Co^{I}H}$. The peak corresponding to the reduction potential $E^{\circ}_{Co^{III}H/Co^{II}H}$ may not be observed experimentally because it is buried under other catalytic peaks in this region, such as the peak corresponding to $E^{\circ}_{Co^{II}/Co^{I}}$. Thus, this computational approach is able to assist in the assignment of ambiguous peaks in the cyclic voltammetry experiments.

Analogous isodesmic reactions with the same reference reactions given in eq 4 were used to calculate reduction potentials for $Co(dpgBF_2)_2$. The calculated values of $E^{\circ}_{Co^{II}/Co^{I}}$ = −0.27 V vs SCE and $E^{\circ}_{Co^{III}/Co^{II}}$ = 0.26 V vs SCE are in excellent agreement with the experimental values of −0.28 V vs SCE and ~0.3 V vs SCE, respectively. Note that the references in the isodesmic reactions contain $dmgBF_2$ and dppe ligands, and no references contain $dpgBF_2$ ligands. The excellent agreement of the calculated reduction potentials with experimental data for the $Co(dpgBF_2)_2$ complexes provides further validation of the computational methodology and indicates that this approach can be used to predict the reduction potentials and pK_as for a range of cobaloximes without utilizing additional experimental data. Thus, we are able to examine the effects of ligand modification on the thermodynamic properties of the catalysts.

A comparison of the calculated and experimental pK_a values is provided in Table 5. The calculated pK_a of $Co^{III}H(dmgBF_2)_2$ agrees with the experimental value by construction in the isodesmic reactions. The calculated pK_a of $Co^{II}H(dmgBF_2)_2^-$ differs from the experimental value by 2.8 pK_a units. The experimental pK_as were estimated from simulated cyclic voltammograms that reproduce experimental reduction potentials,[5] and errors in both experiment and theory could contribute to this discrepancy. Most important for the present analysis, our calculated pK_as follow the qualitative trend in acidity for the Co−hydride complexes with respect to each other. Specifically, the pK_a is greater for $Co(II)H^-$ than for Co(III)H for both cobaloximes, as expected based on electrostatic considerations. In addition, the pK_a values of $Co(dmgBF_2)_2$ are greater than those of $Co(dpgBF_2)_2$. This result is consistent with the experimental observation that hydrogen evolution requires a stronger acid for the $Co(dpgBF_2)_2$ catalysts than for the $Co(dmgBF_2)_2$ catalysts.[4,10]

III.C. Reorganization Energies for Electron Transfer. The inner-sphere and heterogeneous solvent reorganization energies for the electron transfer steps are provided in Table 6. The heterogeneous solvent reorganization energies were calculated with the dielectric continuum model described above. The results in Table 6 indicate that the heterogeneous solvent reorganization energy is ~0.44 eV, regardless of the particular geometry, oxidation state, or axial ligand structure of the molecule. This consistency arises because the overall size of the cobalt complex is not strongly influenced by any of these factors. Note that our computational approach may underestimate the solvent reorganization energy because the molecule is assumed to be directly on the electrode, and the solvent reorganization energy increases as the distance between the molecule and the electrode increases.

The inner-sphere reorganization energies were calculated with eq 9 and also with eq 10 when ligand loss is thought to occur during reduction. The contribution to the inner-sphere reorganization energy due to ligand loss is depicted graphically in terms of a free energy barrier in Figure S1, Supporting Information.

dx.doi.org/10.1021/ic201842v |Inorg. Chem. 2011, 50, 11252–11262

Table 7. Reaction Free Energies for Proton Transfer and Hydrogen Production Steps in $Co(dmgBF_2)_2$ Complexes[a]

proton transfer[b]	$Co(I)^-$ + HA	$Co(0)^{2-}$ + HA
CF_3COOH	−0.038	−0.45
$TsOH \cdot H_2O$	−0.31	−0.72
$HBF_4 \cdot Et_2O$	−0.78	−1.19
monometallic H_2 production[c]	Co(III)H + HA	$Co(II)H^-$ + HA
CF_3COOH	0.70	−0.029
$TsOH \cdot H_2O$	0.43	−0.30
$HBF_4 \cdot Et_2O$	−0.042	−0.77
bimetallic H_2 production[d]	Co(III)H + Co(III)H	$Co(II)H^-$ + $Co(II)H^-$
	−0.007	0.026

[a] Values given in eV in acetonitrile. The pK_a values for the three acids were determined experimentally and are 12.7, 8.0, and 0.1 for CF_3COOH, $TsOH \cdot H_2O$, and $HB_4 \cdot Et_2O$, respectively, as given in ref 4. [b] The proton is transferred from HA to the Co complex. [c] The acid provides a proton, and the Co−hydride provides a hydride to create H_2. [d] Each Co−hydride provides a hydrogen to create H_2.

We emphasize that this approach provides only a qualitative estimate of this portion of the inner-sphere reorganization energy and may overestimate it. In addition, the electron transfer and associated ligand loss may occur by either a stepwise or a concerted mechanism. For a stepwise mechanism, the contribution to the inner-sphere reorganization energy due to ligand loss does not impact the free energy barrier for the electron transfer step. As a result, the reorganization energies due to ligand loss are given in parentheses in Table 6.

To compare with experiment, we calculated the homogeneous solvent reorganization energies and the inner-sphere reorganization energies (neglecting the effects of ligand loss) for the self-exchange electron transfer reactions, $Co^{III/II}(dpgBF_2)_2$ and $Co^{II/I}(dpgBF_2)_2$. The calculated values, which are presented in Table S3, Supporting Information, are in qualitative agreement with the estimated total reorganization energies based on experimental self-exchange rate constants.[11] This agreement suggests that these computational methods provide qualitatively reasonable reorganization energies.

We analyzed the various contributions to the inner-sphere reorganization energies for the $Co(dmgBF_2)_2$ systems. Qualitatively, the inner-sphere reorganization energy, λ_i, which accounts for solute rearrangements in the absence of ligand loss, decreases as the number of axial acetonitrile ligands decreases. Note that this inner-sphere reorganization energy is calculated in the absence of the ligand when ligand loss occurs during the reduction. For the $Co^{III}L_2/Co^{II}L_2$ reduction, the relatively large inner-sphere reorganization energy is attributed to a geometrical rearrangement of the acetonitrile ligands from a $Co-N_{nitrile}-C$ angle of 175° to an angle of 147°, as illustrated in Figure 1. For the $Co^{II}L_2/Co^{I}L$ reduction, the moderate inner-sphere reorganization energy is attributed to the shift of the cobalt atom out of the $dmgBF_2$ plane as the $Co-N_{nitrile}$ bond shortens. For the $Co^{I}L/Co^{0}$, $Co^{III}HL/Co^{II}H$, and $Co^{II}H/Co^{I}H$ reductions, the relatively small inner-sphere reorganization energies are attributed to the lack of any significant geometrical rearrangement; no axial acetonitrile ligand is bound in these calculations. For the three reduction reactions that involve ligand loss for $Co(dmgBF_2)_2$, the direct contribution of ligand loss to the inner-sphere reorganization energy is ~0.56 eV. As mentioned above, this approach may overestimate the contribution of ligand loss to the inner-sphere reorganization energy. If the electron transfer and associated ligand loss occur via a concerted mechanism, the total inner-sphere reorganization energies for $Co^{III}L_2/Co^{II}L_2$ and $Co^{II}L_2/Co^{I}L$ are similar because the large contribution of the $Co^{III}L_2/Co^{II}L_2$ structural rearrangement to the inner-sphere reorganization energy is similar to the sum of the contributions from the moderate $Co^{II}L_2/Co^{I}L$ structural rearrangement and dissociation of an axial acetonitrile ligand. If the electron transfer and associated ligand loss occur via a sequential mechanism, however, the contribution due to ligand loss does not impact the free energy barrier for the electron transfer step, and the inner-sphere reorganization energy for the electron transfer step is greater for $Co^{III}L_2/Co^{II}L_2$ than for $Co^{II}L_2/Co^{I}L$.

The reaction free energies for the proton transfer and hydrogen production steps with three different acids are provided in Table 7. These reaction free energies were calculated from the thermodynamic equations provided in Scheme S1, Supporting Information. Note that this table provides only thermodynamic quantities (i.e., the relative free energies of the reactants and products) and does not provide the free energy barriers of the reactions. The proton transfer reactions from the acid, HA, to the $Co(I)^-$ and $Co(0)^{2-}$ complexes are exoergic for all three acids considered, where protonation of the cobalt complex becomes more thermodynamically favorable as the pK_a of the acid decreases. Protonation of the $Co(0)^{2-}$ complex is more thermodynamically favorable than protonation of the $Co(I)^-$ complex, as expected based on electrostatic considerations. For the monometallic hydrogen production step, the free energy of reaction decreases as the pK_a of the acid decreases and is greater for Co(III)H than for $Co(II)H^-$, as expected based on electrostatic considerations for removal of a hydride, H^-. For the bimetallic hydrogen production step, the free energy of reaction is nearly identical for Co(III)H and $Co(II)H^-$, indicating that removal of a neutral hydrogen atom is thermodynamically similar for the two oxidation states of cobalt in these complexes. Note that the free energy barriers for these two bimetallic hydrogen production steps may differ significantly, and the work term required to bring the two cobalt complexes together will be greater for $Co(II)H^-$ than for Co(III)H due to the electrostatic repulsion.

III.D. Comparison of Reaction Pathways. The individual steps in the six reaction pathways considered here are given in Scheme 1, where A corresponds to the monometallic pathway and B corresponds to the bimetallic pathway. The equations used to calculate the free energy of reaction for each step are given in Scheme S1, Supporting Information. Figure 2 depicts the free energy diagrams corresponding to the six reaction pathways for $Co(dmgBF_2)_2$ and *p*-toluenesulfonic acid (tosic acid) with respect to the HA/H_2 couple in acetonitrile. Each cycle starts with $Co^{II}(dmgBF_2)_2$, which is considered to be the resting state of the cobaloxime in the catalytic cycle. The monometallic and bimetallic pathways are denoted in red and blue, respectively. In this figure, the reference is $E^{\circ}_{HA/H_2} = E^{\circ}_{H^+/H_2} - 0.059pK_a(HA) = -0.23$ V vs SCE, corresponding to the half-reaction $HA + e^- \rightarrow (1/2)H_2 + A^-$, where HA is tosic acid with $pK_a = 8.0$ in acetonitrile[4] and $E^{\circ}_{H^+/H_2} = 0.24$ V vs SCE in acetonitrile.[4,30−33] Reduction of HA to H_2 cannot occur at less negative potentials than this reference potential, E°_{HA/H_2}.[33] Moreover, the most effective catalysts are expected to operate at potentials as close as possible to this reference potential. Thus, the optimal pathway

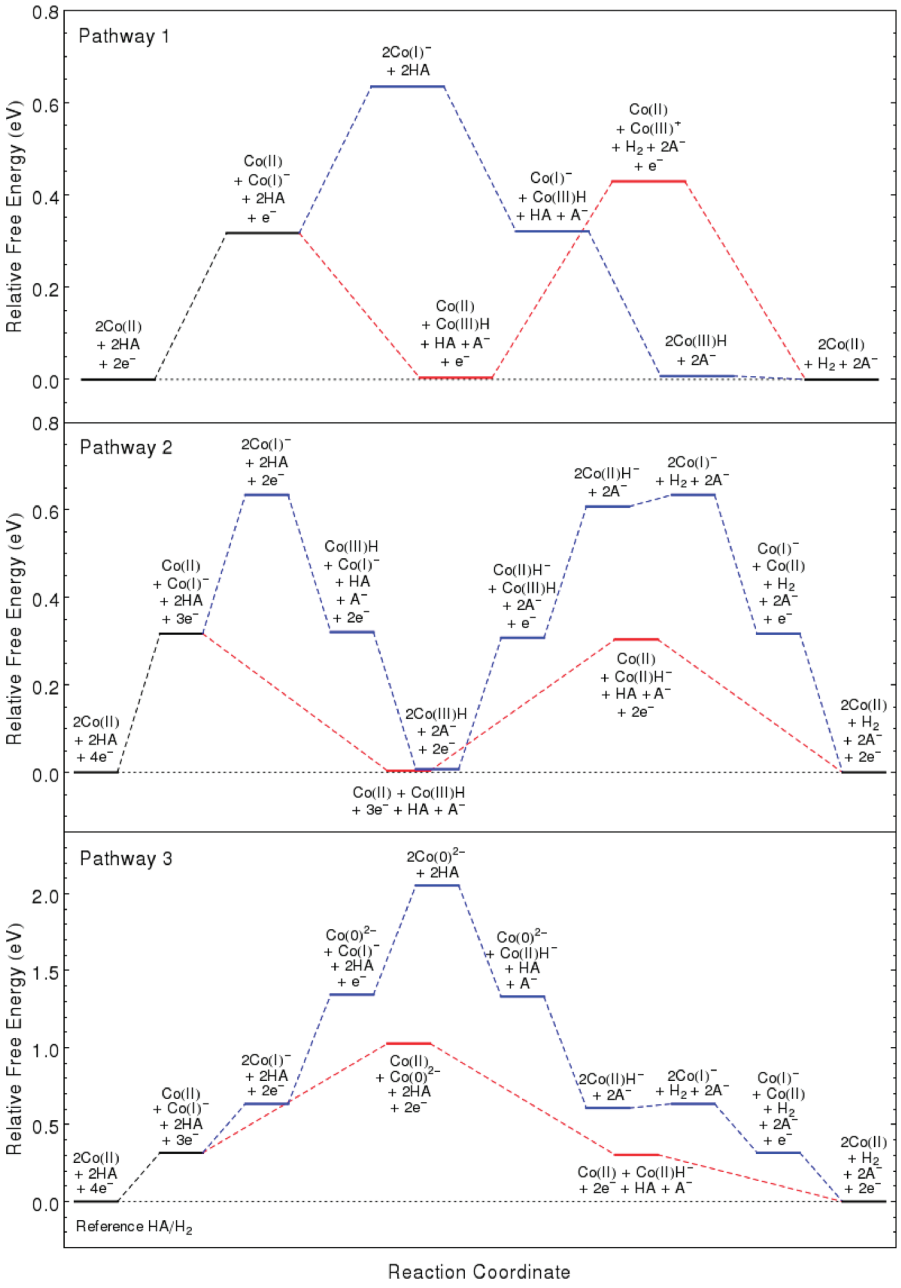

Figure 2. Free energy diagrams for Pathways 1A, 2A, and 3A (monometallic mechanisms, denoted by red lines) and 1B, 2B, and 3B (bimetallic mechanisms, denoted by blue lines) in acetonitrile. Black lines denote states that are applicable to both monometallic and bimetallic pathways. Relative free energies for half reactions corresponding to electron transfer are calculated with respect to the HA/H_2 couple in acetonitrile. In this diagram, HA is $TsOH \cdot H_2O$ ($pK_a = 8.0$). The free energy barriers are not shown.

will avoid large deviations (i.e., low minima or high maxima) from this reference potential. The same free energy diagrams are presented in Figure 3 at the electrode potential corresponding to the Co^{II}/Co^{I} couple (i.e., with a reference potential of $E^{o}_{Co^{II}/Co^{I}} = -0.55$ V vs SCE). This figure illustrates the pathways under typical experimental conditions for these electrocatalysts, where H_2 evolution was found to occur at electrode potentials just negative of $E^{o}_{Co^{II}/Co^{I}}$.[4]

In this paper, we present a thermodynamic analysis of these pathways, considering the free energy change for each step of the various pathways. The free energy barriers for electron transfer may be calculated from the Marcus theory expression in eq 8 using the corresponding reduction potentials and reorganization energies, but this calculation would require the assumption of a concerted or sequential mechanism for the ligand loss associated with some of the electron transfer steps. Moreover, a kinetic analysis of the various mechanistic pathways would also require calculation of the free energy barriers for the proton transfer and hydrogen production steps. Such a study would necessitate consideration of the effects of hydrogen tunneling in the proton transfer reactions. When water is present, the possibility of solvent-mediated proton transfer should also be considered. Moreover, the overall rates for the proposed pathways will depend on the concentrations of the cobaloxime and acid.

dx.doi.org/10.1021/ic201842v |*Inorg. Chem.* 2011, 50, 11252–11262

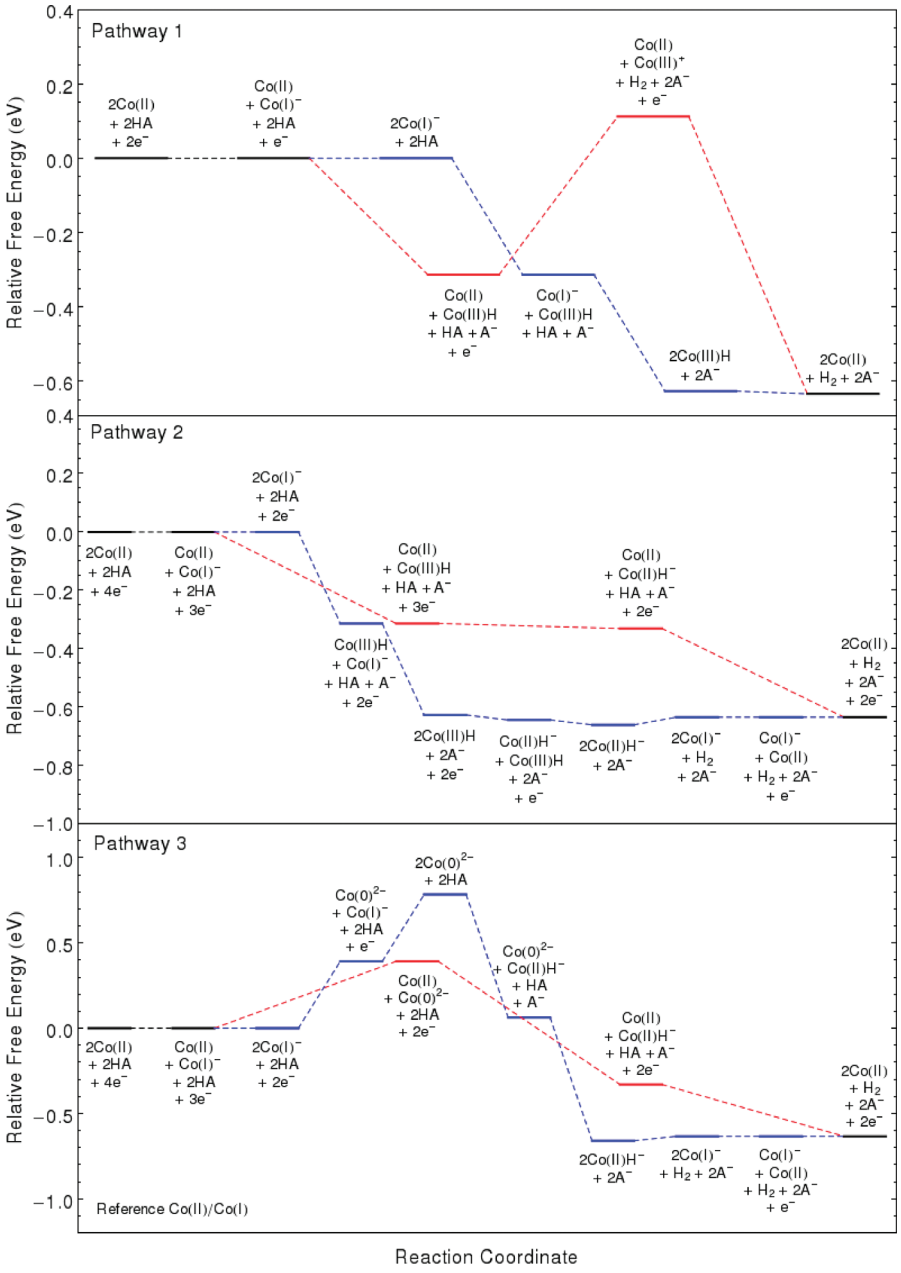

Figure 3. Free energy diagrams for Pathways 1A, 2A, and 3A (monometallic mechanisms, denoted by red lines) and 1B, 2B, and 3B (bimetallic mechanisms, denoted by blue lines) in acetonitrile. Black lines denote states that are applicable to both monometallic and bimetallic pathways. Relative free energies for half reactions corresponding to electron transfer are calculated with respect to the Co^{II}/Co^{I} couple in acetonitrile. In this diagram, HA is $TsOH \cdot H_2O$ (pK_a = 8.0). The free energy barriers are not shown.

This type of kinetic analysis is beyond the scope of the present work. We also point out that the reduction potentials and pK_as provided in the previous subsections may be used to generate analogous free energy diagrams for $Co(dpgBF_2)_2$ and for other acids. A similar thermodynamic analysis could be applied to these systems.

According to our calculations, Pathway 2A is the thermodynamically preferred mechanism for the monometallic mechanisms (denoted in red in Figures 2 and 3). This preference is clear from Figure 3, which indicates that Pathway 2A is the only monometallic mechanism for which all steps are exoergic at the electrode potential corresponding to the Co^{II}/Co^{I} couple. Moreover, Figure 2 illustrates that the maximum free energy of any state relative to E^{o}_{HA/H_2} is lowest for Pathway 2A. The most negative reduction potential for electron transfer, corresponding to the Co^{II}/Co^{I} reduction, is the same for Pathways 1A and 2A. The reaction free energy for the hydrogen production step with tosic acid, however, is 0.43 eV for Pathway 1A and −0.30 eV for Pathway 2A. As discussed above and indicated by the reaction free energies given in Table 7, removal of a hydride from $Co(II)H^{-}$ is thermodynamically favored over removal of a hydride from Co(III)H. Pathway 3A is thermodynamically unfavorable because of the Co^{I}/Co^{0} reduction, which is associated with a significantly more negative reduction potential than is the Co^{II}/Co^{I} reduction. Pathways including the $Co^{II}H/Co^{I}H$ reduction were not considered because of its even more negative reduction potential.

dx.doi.org/10.1021/ic201842v |*Inorg. Chem.* 2011, 50, 11252–11262

Among the bimetallic pathways (denoted in blue in Figures 2 and 3), Pathways 1B and 2B are both feasible and similar from the thermodynamic perspective. Figure 3 indicates that Pathways 1B and 2B correspond to mechanisms for which all steps are exoergic or only slightly endoergic at the electrode potential corresponding to the Co^{II}/Co^{I} couple. As shown in Figure 2, the maximum free energy of any state relative to E°_{HA/H_2} is similar for these two pathways. The reaction free energy for the bimetallic hydrogen production step is −0.007 eV for Pathway 1B and 0.026 eV for Pathway 2B. The difference between these values is smaller than the errors associated with the computational methods. Pathway 3B is thermodynamically unfavorable because of the Co^{I}/Co^{0} reduction, as in Pathway 3A. Without information regarding the free energy barriers to the proton transfer and hydrogen production steps, differentiating between Pathways 1B and 2B is difficult. As mentioned above, however, the work term required to bring the two cobalt complexes together in acetonitrile solution will be greater for $Co(II)H^{-}$ than for Co(III)H due to the electrostatic repulsion. On the basis of this electrostatic work term, Pathway 1B is the preferred bimetallic pathway.

These various mechanistic pathways have been examined in the context of both electrochemical and photochemical experiments on cobaloximes. The cyclic voltammetry experiments of Hu, Brunschwig, and Peters[4] supported a bimetallic mechanism, but these authors pointed out that direct kinetic evidence is still needed. These authors also suggested that the monometallic mechanism is expected to become more important for very strong acids and/or complexes with a relatively negative Co^{III}/Co^{II} potential. According to Fontecave and co-workers,[5] Pathway 1 is favored for strong acids, Pathway 2 is favored for lower strength acids, and Pathway 3 is favored for very weak acids. Their electrochemical studies indicated that Pathway 1 occurs via the monometallic mechanism, but they could not distinguish between the monometallic and bimetallic mechanisms for Pathways 2 and 3. The photochemical experiments of Eisenberg and co-workers[7] supported the monometallic mechanism. These authors favored Pathway 2 because of the alternation of electron and proton transfer in this mechanism. In photochemical studies, Dempsey, Winkler, and Gray[11] considered both the monometallic and bimetallic mechanisms of Pathway 1 and favored the bimetallic mechanism because of unfavorable reaction free energies and high barriers for electron transfer in the monometallic mechanism. These authors also pointed out that the monometallic mechanism will dominate at very high acid concentrations. The transient absorption measurements in ref 13 are consistent with Pathway 2A, which is the thermodynamically preferred monometallic pathway according to our calculations.

On the basis of all of these analyses, the preferred pathway may differ for the electrochemical and photochemical processes and depends on the acid strength and concentration as well as the potentials of the cobaloximes, which can be tuned by modifying the ligands. The theoretical approach presented in this paper provides the free energy diagrams for any specified cobaloxime catalyst and acid. Analysis of these free energy diagrams in terms of the overpotential required in electrochemical processes or the excitation energy in photochemical processes will provide insight into the preferred pathways. Note that steric and electrostatic effects in the H_2 production steps may also play a role in differentiating the monometallic and bimetallic mechanisms and will be considered in future work. In addition, calculation of free energy barriers for the proton transfer and H_2 production steps, as well as investigation of concerted proton-coupled electron transfer mechanisms,[52,53] are directions for future research.

IV. CONCLUSIONS

In this paper, we presented a computational study of the $Co(dmgBF_2)_2$ and $Co(dpgBF_2)_2$ hydrogen evolving catalysts. Comparison of the calculated reduction potentials to experimentally determined values indicates that this approach provides quantitatively accurate relative reduction potentials for these types of catalysts. Comparison to pK_a values and reorganization energies that were estimated based on experimental data suggests that this approach provides at least qualitatively accurate predictions of these quantities as well. Moreover, this computational study assisted in the assignment of an ambiguous peak in the cyclic voltammetry experiments for $Co(dmgBF_2)_2$. Previously, a peak measured at ca. −1.0 V vs SCE was tentatively assigned to the reduction potential $E^{\circ}_{Co^{III}H/Co^{II}H}$,[4] but our calculations suggest that this transition is more likely to correspond to the reduction potential $E^{\circ}_{Co^{II}H/Co^{I}H}$ in protic solution. We also predicted the pK_a values of the Co−hydride complexes and other reduction potentials that have not been determined experimentally for both $Co(dmgBF_2)_2$ and $Co(dpgBF_2)_2$.

In addition, this computational study has provided mechanistic insight that cannot be deduced directly from the electrochemical experiments. Specifically, we determined whether the axial acetonitrile ligands are present for each intermediate along the reaction pathway. Our calculations are consistent with a mechanism in which the Co(III) and Co(II) complexes have two axial solvent ligands and the Co(I) complex has a single axial ligand along the reaction pathway. Furthermore, we generated the free energy diagrams for six different monometallic and bimetallic hydrogen production pathways and identified the most favorable pathways for $Co(dmgBF_2)_2$ and tosic acid. Our calculations suggest that Pathway 2A, in which a Co(II)H intermediate reacts with the acid to produce H_2, is the thermodynamically favorable monometallic pathway. Pathways 1B and 2B, in which either two Co(III)H or two Co(II)H complexes react to produce H_2, are both thermodynamically feasible bimetallic pathways, but Pathway 1B is favored according to the electrostatic work term associated with bringing the two cobalt complexes together in solution. The preference between the monometallic and the bimetallic pathways depends on the relative concentrations of the acid and the cobaloxime catalyst. Specifically, the monometallic pathway is favored at very high acid concentrations. This mechanistic insight, as well as the ability to predict the impact of modifying the ligands or acid on the energetics of the various pathways, is important for designing more effective catalysts for solar energy conversion.

■ ASSOCIATED CONTENT

Supporting Information. Comparison of bond lengths for $Co(dmgBF_2)_2$ calculated with B3LYP and B3P86 functionals; comparison of reduction potentials with varying axial ligands along reaction pathway for $Co(dmgBF_2)_2$; homogeneous reorganization energies for self-exchange reactions of $Co(dpgBF_2)_2$; illustration of ligand loss contribution to inner-sphere reorganization energy for $Co^{II}(dmgBF_2)_2L_2/Co^{I}(dmgBF_2)_2L^{-}$ reduction; coordinates

dx.doi.org/10.1021/ic201842v |Inorg. Chem. 2011, 50, 11252–11262

and energies of optimized structures. This material is available free of charge via the Internet at http://pubs.acs.org.

AUTHOR INFORMATION

Corresponding Authors
*E-mail: shs@chem.psu.edu.

ACKNOWLEDGMENT

We are very grateful to Alexander Soudackov, Samantha Horvath, and Jay Winkler for useful discussions and helpful advice. This work was supported by the NSF Center for Chemical Innovation (Powering the Planet, grant CHE-0947829).

REFERENCES

(1) Connolly, P.; Espenson, J. H. *Inorg. Chem.* **1986**, *25*, 2684–2688.
(2) Hu, X.; Cossairt, B. M.; Brunschwig, B. S.; Lewis, N. S.; Peters, J. C. *Chem. Commun.* **2005**, 4723–4725.
(3) Razavet, M.; Artero, V.; Fontecave, M. *Inorg. Chem.* **2005**, *44*, 4786–4795.
(4) Hu, X.; Brunschwig, B. S.; Peters, J. C. *J. Am. Chem. Soc.* **2007**, *129*, 8988–8998.
(5) Baffert, C.; Artero, V.; Fontecave, M. *Inorg. Chem.* **2007**, *46*, 1817–1824.
(6) Du, P.; Knowles, K.; Eisenberg, R. *J. Am. Chem. Soc.* **2008**, *130*, 12576–12577.
(7) Du, P.; Schneider, J.; Luo, G.; Brennessel, W. W.; Eisenberg, R. *Inorg. Chem.* **2009**, *48*, 4952–4962.
(8) Lazarides, T.; McCormick, T.; Du, P.; Luo, G.; Lindley, B.; Eisenberg, R. *J. Am. Chem. Soc.* **2009**, *131*, 9192–9194.
(9) Jacques, P.-A.; Artero, V.; Pécaut, J.; Fontecave, M. *Proc. Natl. Acad. Sci. U.S.A.* **2009**, *106*, 20627–20632.
(10) Dempsey, J. L.; Brunschwig, B. S.; Winkler, J. R.; Gray, H. B. *Acc. Chem. Res.* **2009**, *42*, 1995–2004.
(11) Dempsey, J. L.; Winkler, J. R.; Gray, H. B. *J. Am. Chem. Soc.* **2010**, *132*, 1060–1065.
(12) Szajna-Fuller, E.; Bakac, A. *Eur. J. Inorg. Chem.* **2010**, 2488–2494.
(13) Dempsey, J. L.; Winkler, J. R.; Gray, H. B. *J. Am. Chem. Soc.* **2010**, *132*, 16774–16776.
(14) Kelly, C. P.; Cramer, C. J.; Truhlar, D. G. *J. Phys. Chem. B* **2007**, *111*, 408–422.
(15) Qi, X.-J.; Fu, Y.; Liu, L.; Guo, Q.-X. *Organometallics* **2007**, *26*, 4197–4203.
(16) Tsai, M.-K.; Rochford, J.; Polyansky, D. E.; Wada, T.; Tanaka, K.; Fujita, E.; Muckerman, J. T. *Inorg. Chem.* **2009**, *48*, 4372–4383.
(17) Wang, T.; Brudvig, G. W.; Batista, V. S. *J. Chem. Theory Comput.* **2010**, *6*, 2395–2401.
(18) Chen, S.; Raugei, S.; Rousseau, R.; Dupuis, M.; Bullock, R. M. *J. Phys. Chem. A* **2010**, *114*, 12716–12724.
(19) Liu, Y. P.; Newton, M. D. *J. Phys. Chem.* **1994**, *98*, 7162–7169.
(20) Klimkans, A.; Larson, S. *Chem. Phys.* **1994**, *189*, 25–31.
(21) Savéant, J. M. *J. Am. Chem. Soc.* **1987**, *109*, 6788–6795.
(22) Costentin, C.; Robert, M.; Savéant, J.-M. *Chem. Phys.* **2006**, *324*, 40–56.
(23) Marcus, R. A. *Annu. Rev. Phys. Chem.* **1964**, *15*, 155–196.
(24) Marcus, R. A.; Sutin, N. *Biochim. Biophys. Acta* **1985**, *811*, 265–322.
(25) Roy, L. E.; Jakubikova, E.; Guthrie, M. G.; Batista, E. R. *J. Phys. Chem. A* **2009**, *113*, 6745–6750.
(26) Lim, C.; Bashford, D.; Karplus, M. *J. Phys. Chem.* **1991**, *95*, 5610–5620.
(27) Himmel, D.; Gollo, S. K.; Leito, I.; Krossing, I. *Angew. Chem., Int. Ed.* **2010**, *49*, 6885–6888.
(28) Bartmess, J. E. *J. Phys. Chem.* **1994**, *98*, 6420–6424.
(29) Ciancanelli, R.; Noll, B. C.; DuBois, D. L.; DuBois, M. R. *J. Am. Chem. Soc.* **2002**, *124*, 2984–2992.
(30) Connelly, N. G.; Geiger, W. E. *Chem. Rev.* **1996**, *96*, 877–910.
(31) Pavlishchuk, V. V.; Addison, A. W. *Inorg. Chim. Acta* **2000**, *298*, 97–102.
(32) Daniele, S.; Ugo, P.; Mazzocchin, G.-A. *Anal. Chim. Acta* **1985**, *173*, 141–148.
(33) Felton, G. A. N.; Glass, R. S.; Lichtenberger, D. L.; Evans, D. H. *Inorg. Chem.* **2006**, *45*, 9181–9184.
(34) Frisch, M. J.; Trucks, G. W.; Schlegel, H. B.; Scuseria, G. E.; Robb, M. A.; Cheeseman, J. R.; Scalmani, G.; Barone, V.; Mennucci, B.; Petersson, G. A.; Nakatsuji, H.; Caricato, M.; Li, X.; Hratchian, H. P.; Izmaylov, A. F.; Bloino, J.; Zheng, G.; Sonnenberg, J. L.; Hada, M.; Ehara, M.; Toyota, K.; Fukuda, R.; Hasegawa, J.; Ishida, M.; Nakajima, T.; Honda, Y.; Kitao, O.; Nakai, H.; Vreven, T.; J. A. Montgomery, J.; Peralta, J. E.; Ogliaro, F.; Bearpark, M.; Heyd, J. J.; Brothers, E.; Kudin, K. N.; Staroverov, V. N.; Kobayashi, R.; Normand, J.; Raghavachari, K.; Rendell, A.; Burant, J. C.; Iyengar, S. S.; Tomasi, J.; Cossi, M.; Rega, N.; Millam, J. M.; Klene, M.; Knox, J. E.; Cross, J. B.; Bakken, V.; Adamo, C.; Jaramillo, J.; Gomperts, R.; Stratmann, R. E.; Yazyev, O.; Austin, A. J.; Cammi, R.; Pomelli, C.; Ochterski, J. W.; Martin, R. L.; Morokuma, K.; Zakrzewski, V. G.; Voth, G. A.; Salvador, P.; Dannenberg, J. J.; Dapprich, S.; Daniels, A. D.; Farkas, Ö.; Foresman, J. B.; Ortiz, J. V.; Cioslowski, J.; Fox, D. J. *Gaussian 09*, Revision B.1; Gaussian, Inc.: Wallingford, CT, 2009.
(35) Becke, A. D. *J. Chem. Phys.* **1993**, *98*, 5648–5652.
(36) Perdew, J. P. *Phys. Rev. B* **1986**, *33*, 8822–8824.
(37) McLean, A. D.; Chandler, G. S. *J. Chem. Phys.* **1980**, *72*, 5639–5648.
(38) Krishnan, R.; Binkley, J. S.; Seeger, R.; Pople, J. A. *J. Chem. Phys.* **1980**, *72*, 650.
(39) Wachters, A. J. H. *J. Chem. Phys.* **1970**, *52*, 1033–1036.
(40) Hay, P. J. *J. Chem. Phys.* **1977**, *66*, 4377–4384.
(41) Raghavachari, K.; Trucks, G. W. *J. Chem. Phys.* **1989**, *91*, 1062–1065.
(42) Hehre, W. J.; Ditchfield, R.; Pople, J. A. *J. Chem. Phys.* **1972**, *56*, 2257–2261.
(43) Barone, V.; Cossi, M. *J. Phys. Chem. A* **1998**, *102*, 1995–2001.
(44) Cossi, M.; Rega, N.; Scalmani, G.; Barone, V. *J. Comput. Chem.* **2003**, *24*, 669–681.
(45) Bondi, A. *J. Phys. Chem.* **1964**, *68*, 441.
(46) Floris, F.; Tomasi, J. *J. Comput. Chem.* **1989**, *10*, 616–627.
(47) Floris, F. M.; Tomasi, J.; Ahuir, J. L. P. *J. Comput. Chem.* **1991**, *12*, 784–791.
(48) Pierotti, R. A. *Chem. Rev.* **1976**, *76*, 717–726.
(49) Lee, C.; Yang, W.; Parr, P. G. *Phys. Rev. B* **1988**, *37*, 785–789.
(50) Marcus, R. A. *J. Chem. Phys.* **1956**, *24*, 966–978.
(51) Marcus, R. A. *J. Chem. Phys.* **1965**, *43*, 679–701.
(52) Hammes-Schiffer, S.; Soudackov, A. V. *J. Phys. Chem. B* **2008**, *112*, 14108–14123.
(53) Hammes-Schiffer, S.; Stuchebrukhov, A. A. *Chem. Rev.* **2010**, *110*, 6939–6960.